Journal for ImmunoTherapy of Cancer

Neutrophil extracellular traps impede cancer metastatic seeding via protease-activated receptor 2-mediated downregulation of phagocytic checkpoint CD24

Yu Liu,[1] Jianhui Ma,[1] Yiming Ma,[1] Bing-zhi Wang,[2] Yinong Wang,[1] Junhu Yuan,[1] Fanyu Zhang,[1] Xinhua Zhao,[1] Kun Chen ,[3,4] Xiaoli Zhang,[5] Hongying Wang [1]

To cite: Liu Y, Ma J, Ma Y, *et al*. Neutrophil extracellular traps impede cancer metastatic seeding via protease-activated receptor 2-mediated downregulation of phagocytic checkpoint CD24. *Journal for ImmunoTherapy of Cancer* 2025;**13**:e010813. doi:10.1136/jitc-2024-010813

► Additional supplemental material is published online only. To view, please visit the journal online (https://doi.org/10.1136/jitc-2024-010813).

YL and JM contributed equally.

Accepted 10 February 2025

For numbered affiliations see end of article.

Correspondence to
Dr Hongying Wang;
hongyingwang@cicams.ac.cn

ABSTRACT

Background Phagocytic clearance by macrophages represents a critical immune surveillance mechanism in cancer liver metastasis. Neutrophils, the most abundant immune cells encountered by cancer cells in circulation, play key roles in metastasis through neutrophil extracellular traps (NETs). Although NETs promote macrophage phagocytosis during infection, whether they regulate phagocytosis during cancer metastasis is unknown. The present study aimed to explore the roles of NETs in regulating macrophage phagocytosis during the seeding process of liver metastasis and the mechanisms underlying the roles.

Methods A lipopolysaccharide-induced NET model was applied to study the role of NETs on colorectal cancer (CRC) liver metastasis. The neutrophils isolated from human peripheral blood were stimulated with PMA to release NETs, which were collected and added to the cultures of different CRC cell lines for in vitro studies. Macrophage phagocytosis was assessed with flow cytometry in vitro and in vivo. RNA-seq and microRNA array analyses were performed to identify key pathways regulated by NETs and downstream key molecules. The macrophage phenotypes were evaluated using immunohistochemistry, flow cytometry, and cytokine and chemokine arrays.

Results NETs promote macrophage phagocytosis both in vitro and in vivo. Neutrophil elastase (NE), which was able to inactivate the canonical signal of protease-activated receptor 2 (PAR2), downregulated the phagocytotic checkpoint CD24. Notably, PAR2 deficiency imitated the effect of NETs on phagocytosis and CD24. Mechanistic studies indicated that inhibiting PAR2 expression upregulated miR-34a and miR-146a and downregulated CD24 in cancer cells. In addition, PAR2 depletion enhanced the recruitment and M1 polarization of macrophages by upregulating CSF-1 and CXCL1. The correlation of NETs/NE and CD24 was corroborated using human CRC specimens. Furthermore, PAR2 blockade combined with an anti-EGFR antibody (cetuximab (CTX)) synergistically enhanced the phagocytic ability of macrophages and suppressed liver metastasis in vivo.

Conclusions NET-derived elastase inactivated PAR2 canonical signaling and promoted phagocytosis by downregulating CD24, which functions as a phagocytotic checkpoint in CRC liver metastasis. Thus, PAR2 inhibitors combined with CTX may serve as a novel therapeutic strategy against advanced CRC.

WHAT IS ALREADY KNOWN ON THIS TOPIC

⇒ Phagocytic checkpoints, which regulate phagocytic clearance of cancer cells, are attractive targets for cancer immunotherapy, and their blockade improves the efficacy of antibody therapy significantly. Uncovering the regulatory mechanisms of phagocytosis in the microenvironment during cancer metastasis could provide a novel therapeutic strategy for treating patients with advanced colorectal cancer (CRC).

WHAT THIS STUDY ADDS

⇒ This research revealed that neutrophil extracellular traps (NETs) promote macrophage phagocytosis both in vitro and in vivo. NETs promote phagocytosis by downregulating CD24, which functions as a phagocytic checkpoint in CRC liver metastasis. Protease-activated receptor 2 (PAR2), a G protein-coupled receptor, is a key node that manipulates the ability to initiate tumor formation and evade immune surveillance.

HOW THIS STUDY MIGHT AFFECT RESEARCH, PRACTICE OR POLICY

⇒ PAR2 inhibitors combined with cetuximab may provide a novel therapeutic strategy against advanced CRC. During the metastatic seeding phase, short-term phagocytosis-promoting therapy can achieve significant long-term inhibitory effects on metastasis.

BACKGROUND

Metastasis is the leading cause of cancer-related deaths, with the liver being the main site of metastatic diseases, particularly gastrointestinal malignancies. A myriad of malignant

cells dissociate from the primary site, enter the circulatory system, encounter and overcome numerous challenges, and ultimately, only a few tumor seed cells successfully reach the distal metastatic organ, the liver. On entering the liver, circulating cancer cells face immense pressure from the innate immune system, including macrophages, neutrophils, and natural killer (NK) cells, which play a crucial role in immune surveillance either alone or in coordination.[1–3] Only tumor cells that successfully evade immune clearance can survive and form metastatic foci.

Macrophages are the most abundant innate immune cells in the liver and the first defense mechanism against metastasis. Macrophages, including monocyte-derived and tissue-resident cells, are considered "professional" phagocytes because they migrate toward and efficiently engulf target cells.[4] Macrophages engulf more than 90% of cancer cells within the first few days after arriving in the liver.[5] Therefore, impairment of phagocytosis during the invisible phase of metastatic colonization is critical for preventing and treating metastatic diseases.[6]

Avoiding phagocytosis is a critical mechanism of immune escape during tumor metastasis. Phagocytosis is triggered by "eat me" signals or restrained by "don't eat me" signals that bind to corresponding anti-phagocytic receptors.[7] Overexpression of "don't eat me" molecules is an important immune evasion mechanism in gastrointestinal carcinogenesis.[8] CD47-SIRPα (signal regulatory protein alpha), B2M/LILRB1, and programmed death-ligand 1 (PD-L1)/programmed cell death protein-1 have been characterized as non-eat me checkpoints.[9–11] Interrupting the CD47-SIRPα axis using antibodies reportedly enhances phagocytosis, with marked antitumor effects.[8]

Neutrophils, the most abundant immune cells encountered by cancer cells in circulation, play significant roles in metastasis. As part of the innate immune system, neutrophils in the lung inhibit metastatic seeding of cancer cells through H_2O_2 generation.[12] Recently, however, neutrophils have emerged as metastasis-promoting factors in the liver that capture circulating tumor cells (CTCs) and establish metastatic niches through neutrophil extracellular traps (NETs), which are released by activated neutrophils.[13 14] NETs are extracellular web-like structures consisting of DNA, histones, and granule components, such as myeloperoxidase (MPO) and neutrophil elastase (NE).[15] NETs protect against infection by facilitating the capture and clearance of circulating bacteria by macrophages.[16 17] However, whether they regulate phagocytosis during cancer metastasis remains unknown.

Colorectal cancer (CRC) is a common cancer with high morbidity and mortality rates worldwide. The liver is the most common target organ for CRC metastasis and the main cause of mortality.[2] Once metastasis occurs, the 5-year survival rate is below 20%. Chemotherapy is the primary treatment for patients with unresectable advanced CRC. Although immunotherapy (immune checkpoint blockade) has shown considerable success in treating various cancers, its efficacy against CRC appears limited.[18 19] Uncovering the mechanisms underlying immune evasion will provide a novel therapeutic opportunity for treating patients with metastatic CRC. Thus, in the present study, we aimed to investigate the role of NETs in regulating macrophage-mediated immune surveillance during liver metastasis of CRC.

METHODS

Human specimens and cell lines

Peripheral blood and CRC tumor samples were obtained from healthy donors (n=23) and patients (n=37 or n=32) who underwent resection of CRC at the Chinese Academy of Medical Sciences, Cancer Hospital (Beijing, China) from June 2019 to December 2022. All the patients had not received chemotherapy or radiotherapy before the surgery. Informed consent was obtained from all patients.

CRC cell lines (HT-29 and SW620), HEK-293T cells, and THP-1 cells were purchased from American Type Culture Collection (Manassas, Virginia, USA). Detailed information is presented in the online supplemental material.

Animal models

6–8 weeks old BALB/c nude mice were purchased from HFK Bioscience (Beijing, China).

Lipopolysaccharide-induced NET formation in mice

BALB/c nude mice were divided randomly into four groups (n=20). Lipopolysaccharide (LPS) (Sigma, 2.5 µg/mouse, Cat# L2630) was intraperitoneally (i.p.) injected to induce systemic inflammation. DNase I (20 µg /mouse, Cat# D5025) was i.p. administered as abrogation 24 hours prior to LPS. Six hours after LPS injection, mice were sacrificed and livers isolated, and a single-cell suspension was prepared for neutrophil infiltration detection using flow cytometry. Mouse liver tissues were fixed with 4% paraformaldehyde and subsequently used for immunofluorescence (IF) staining.[20] For neutrophil depletion assays, mice received one i.p. injection of 1A8 Ly6G antibody (200 mg/mouse) (BE0075-1, Bio X Cell) or rat IgG control (I4131, Sigma) 2 days before LPS injection.

Experimental metastasis in a mouse model of LPS-induced NETs

Six hours after establishment of the LPS-induced NET formation model using BALB/c nude mice, 1×10^6 HT-29 cells stained with pHrodo Deep Red (Thermo Fisher Scientific, Waltham, Massachusetts, USA, Cat# P35357) or HT-29-luciferase cells were injected through the spleen. Livers were removed when mice were euthanized on day 2 of model establishment. Liver tissue was fixed with 4% paraformaldehyde for IF staining or digested into single cells for macrophage detection using flow cytometry. To visualize cancer cells in vivo, mice were i.p. administered 150 mg/kg D-luciferin potassium solution (Beyotime, Cat#196). Subsequently, an IVIS Spectrum System (PerkinElmer, Waltham, Massachusetts, USA) was used to obtain the images for 10 min after luciferin injection. Living Image V.4.0 was used to determine the total

flux. The liver metastatic lesions were directly counted on tissue sections using H&E staining on day 56 of model establishment.

For the tumor treatment experiments, mice were gavaged with 5 mg/kg/day GB88 (Hebei Sundia Meditech, China) for 2 or 5 days. GB88 was ground and resuspended in olive oil supplemented with 0.1% Tween-80. On the day of the cancer cell injection, 25 mg/kg cetuximab (CTX, Merck Millipore, Darmstadt, Germany, Cat# S20171039) was injected once i.p.

Neutrophil isolation

Human neutrophils were isolated from the peripheral blood of healthy donors using Polymorphprep (Serumwerk Bernburg AG, Germany, Cat#1895) according to the manufacturer's instructions. Purity was confirmed by flow cytometry using antibody panels (online supplemental table 5): CD45, CD11b, CD16, and CD66b staining. Results were analyzed using FlowJo V.10.0 (FlowJo LLC, Ashland, Oregon, USA), where the percentage of $CD45^+CD11b^+CD16^+CD66b^+$ cells to $CD45^+$ immune cells was the proportion of mature neutrophils. In culture conditions, neutrophils were resuspended in Roswell Park Memorial Institute (RPMI) 1640 (Hyclone) with 10% fetal bovine serum and cultured in six-well plates at 37°C under 5% CO_2 conditions.

Ex vivo NET formation and preparation

Freshly isolated neutrophils were seeded on six-well plates (1×10^6/well) and stimulated with PMA (100 ng/mL, Cat# P1585; Sigma-Aldrich, St Louis, Missouri, USA), and/or DNase I (1 µg/mL, Sigma-Aldrich), and/or alvelestat (10 µM, MCE, Monmouth Junction, USA; Cat# HY-15651) for 4 hours with or without allowing the formation of NETs. Subsequently, the supernatants were carefully discharged via slow suction and washed twice to eliminate residual PMA, DNase I, or alvelestat without disturbing NETs. Serum-free RPMI 1640 (2 mL) was added to blow the cells down. The supernatant containing NETs was transferred to 15 mL centrifuge tubes and centrifuged at 2400 rpm for 10 min to eliminate cell debris. Isolated NETs were stored at −80°C for further use. The suspension containing NETs was treated with Sivelestat (10 µM, Selleckchem, Houston, Texas, USA; Cat# S8136) at 37°C for 30–45 min and subsequently used to treat CRC cells.

For the in vitro analysis of NETs, neutrophils (1×10^5 cells) were seeded in Lab-Tek II Chamber Slide System 8 Well Glass Slide (Thermo Fisher Scientific, Waltham, Massachusetts, USA) with PMA (100 ng/mL) and DNase I (1 µg/mL). After 4 hours of incubation, neutrophils were fixed with 4% paraformaldehyde for 30 min at room temperature. Subsequently, cells were blocked with 5% goat serum at 37°C for 30 min. Cells were incubated with anti-H3-Cit (1:100, ab5103, Abcam, Cat# ab5103) and anti-MPO (1:100, YM6663, Immunoway Biotechnology, USA, Cat# YM6663) in blocking buffer overnight at 4°C. CY3-conjugated goat anti-mouse (1:200, Servicebio Biotechnology, Wuhan, China) and FITC-conjugated goat anti-rabbit (1:200, Servicebio) secondary antibodies were used for 1 hour at room temperature (online supplemental table 5). Observation and photographing were performed using the fluorescence microscope (Olympus). The percentage of the field of NET formation was determined using Image J (National Institute for Health). Briefly, the areas of structures depicting NET morphology and positive for MPO or total H3-Cit were counted as NETotic cell areas, and the NET area percentages were analyzed as NETotic cell areas divided by total DNA areas. The percentages of NETotic cells were analyzed as previously described.[21]

Ca^{2+} level measurements

As described previously[22]: HEK-293T cells were digested using enzyme-free cell dissociation buffer (Gibco, REF13151-014). Cells were incubated with 5 µL Fluor-4 AM (Beyotime, Beijing, China, Cat#S1060) containing 1 µL pluronic F-127 and 4 µL sulfinpyrazone for 30 min at 37°C and washed twice with the buffer containing 150 mM NaCl, 3.0 mM KCl, 10 mM dextrose, 20 mM HEPES, and 250 mM sulfinpyrazone. Afterward, cells were resuspended in 4 mL of 1.5 mM $CaCl_2$, and treated with Trypsin (2 µg/mL, Cat#HY-129047, MCE) and NE (3 U/mL, Promega, Madison, Wisconsin, USA, Cat# V189A). Ca^{2+} signals were determined using flow cytometry, and the mean fluorescence intensity was calculated at different times.

Phagocytosis assay

The suspension containing NETs isolated from the above-described experiments was used to treat CRC cells for 12 hours. To conduct flow-cytometry-based phagocytosis assays, carboxyfluorescein succinimidyl ester (CFSE, Thermo, Cat# C34554)-labeled CRC cells were co-cultured with THP-1-derived tumor-associated macrophages (TAMs) for 2 hour. Thereafter, anti-CD24 mAb, anti-EGFR mAb (CTX), and isotype controls (10 µg/mL) were added to the co-cultured system (online supplemental table 5). After co-culturing, the cells were stained with an anti-CD11b antibody (online supplemental table 5), and assays were performed using a FACSCalibur flow cytometer (BD Biosciences). The percentage of $CD11b^+CFSE^+$ macrophages in total $CD11b^+$ macrophages was measured as the phagocytic index. To perform a time-lapse live-cell microscopy-based phagocytosis assay, HT-29 cells were labeled with pHrodo Deep Red succinimidyl ester (Thermo).[23] Subsequently, TAMs (5×10^4) were co-cultured with 1×10^5 pHrodo Deep Red^+ HT-29 cells in 24-well plates (Corning Life Sciences). Cell culture plates were incubated in a 37 °C incubator and imaged at half-hour intervals using an Incucyte System (Sartorius, Göttingen, Germany). The first image was generally acquired within 30 min of co-culture: phagocytic index=number of engulfed cells/(number of macrophages/100).

To conduct in vivo phagocytosis analysis, HT-29 cells were labeled with pHrodo Deep Red dye before being injected into the spleen. Thereafter, flow cytometry and

IF staining were used to analyze the number of pHrodo Deep Red$^+$ HT-29 cells. Gating strategies for phagocytic TAMs: Zombie$^-$, CD45$^+$, CD11b$^+$, F480$^+$, PerCP/Cy5.5$^+$. Finally, the percentage of the phagocytic TAMs in total CD11b$^+$F480$^+$ macrophages was calculated: phagocytic index of IF staining=number of pHrodo Deep Red$^+$ HT-29 cells/ (number of macrophages/100).

In vitro assays

In vitro assays, including reverse transcription-quantitative PCR (RT-qPCR) analysis, western blotting, ELISA, immunohistochemistry (IHC) analysis, and flow cytometry analysis are described in the online supplemental material.

Statistical analyses

GraphPad Prism software (V.6.01; GraphPad Software, San Diego, California, USA) was used for statistical analyses. In the figures, data are presented as mean±SD. All data are presented as means±SEM of three independent experiments. Data were analyzed using Student's t-test, and Pearson's correlation analysis was used for expression correlation analyses. Statistical significance was set at $p<0.05$.

We used the ARRIVE1 reporting guidelines.[24] Further details on the materials and methods are presented in the online supplemental material.

RESULTS

NETs promoted the phagocytosis of tumor cells by macrophages in vivo and in vitro

First, we set up the LPS-induced NET model[20] and confirmed neutrophil recruitment and NET formation in mouse liver with flow cytometry and IF staining of the neutrophil markers (MPO and NE) (online supplemental figure 1A, B). Treatment with DNase I, which can digest extracellular DNA, efficiently abolished NET formation in vivo, but had no effect on neutrophil recruitment (online supplemental figure 1A, B). In the liver metastasis model, macrophage phagocytosis in the liver was enhanced in the LPS group on day 2 after intrasplenic injection of CRC HT-29 cells (figure 1A) coupled with an enhancement of macrophage infiltration (figure 1B), suppression of cancer cell colonization at day 2 (figure 1C), and a decrease in the numbers of metastatic nodules at endpoint (figure 1D). All these LPS-related effects were reversed by DNase I treatment (figure 1A–D). Furthermore, neutrophil depletion with anti-Ly6G antibody abolished LPS-enhanced phagocytosis (online supplemental figure 1C, D). These observations strongly indicated the involvement of NETs released by neutrophils in phagocytosis in vivo. To study the direct effect of NETs on macrophage phagocytosis, we collected NETs released by PMA-induced neutrophils, which were isolated from peripheral blood of healthy donors (online supplemental figure 1E, F). After pretreatment with NETs, CRC cells (HT-29 and SW620) were co-cultured with macrophages followed by flow cytometry-based phagocytosis analysis to identify macrophages that had engulfed CFSE-labeled cancer cells. The presence of NETs significantly increased the percentage of CD11b$^+$CSFE$^+$ cells; this was blocked by DNase I treatment (figure 1E). These results strongly imply that NETs effectively promote phagocytosis of cancer cells by macrophages both in vitro and in vivo.

NET-derived elastase reduced CD24 expression via PAR2 in cancer cells

Phagocytosis is highly regulated by checkpoint molecules, also called "don't eat me" signals, including CD47, CD24, B2M, and PD-L1 (CD274).[9–11 25] To explore the mechanism of NET-regulated phagocytosis, we first identified the checkpoint molecules that are predominant in human CRC. Analysis of single-cell RNA-seq data of CRC liver metastasis revealed that *CD47* and *CD24* were specifically enriched in the cancer cell cluster, whereas their receptor genes *SIRPA* and *SIGLEC10*, respectively, were selectively expressed in the TAM cluster (figure 2A). Subsequently, treatment with NETs significantly decreased the expression of CD24 at messenger RNA (mRNA) and protein levels but not CD47 (figure 2B,C and online supplemental figure 2A, B). DNase I treatment effectively restored the expression of CD24 after its downregulation by NETs (figure 2B,C). Moreover, inhibition of CD24 expression using small interface RNA (online supplemental figure 2C–E) or a blocking mAb (clone SN3) (online supplemental figure 2F, G) effectively enhanced the phagocytic capacity of macrophages as measured using a FACS-based assay and automated live-cell microscopy. These indicate that NETs promote phagocytosis by suppressing CD24 expression in CRC cancer cells.

NETs contain abundant serine proteases, such as NE, which can specifically cleave protease-activated receptor 2 (PAR2).[26 27] The latter is widely overexpressed and activated in an autocrine way in CRC cells.[28 29] Interestingly, NE inhibitors (alvelestat and sivelestat) blocked the downregulation of CD24 (figure 2D) as well as the enhancement of phagocytosis (online supplemental figure 3A) induced by NETs in different cells. In addition, NE treatment mimicked the effect of NETs on CD24 expression (figure 2E) and similarly had no effect on CD47 expression (online supplemental figure 3B). Consistent with previous reports,[26 27] NE not only inactivated the PAR2 signal but also blocked its trypsin-induced canonical activation characterized by intracellular calcium signal (figure 2F). Furthermore, stable knockdown of PAR2 (shPAR2) (online supplemental figure 3C, D) decreased the CD24 expression at the mRNA and protein levels (figure 2G,H), without affecting the CD47 expression (online supplemental figure 3E, F). Importantly, PAR2 depletion completely abolished the NET-induced and NE-induced downregulation of CD24 (figure 2I and online supplemental figure 3G), indicating that the downregulation of CD24 by NETs and NE is mediated by PAR2 in CRC cells.

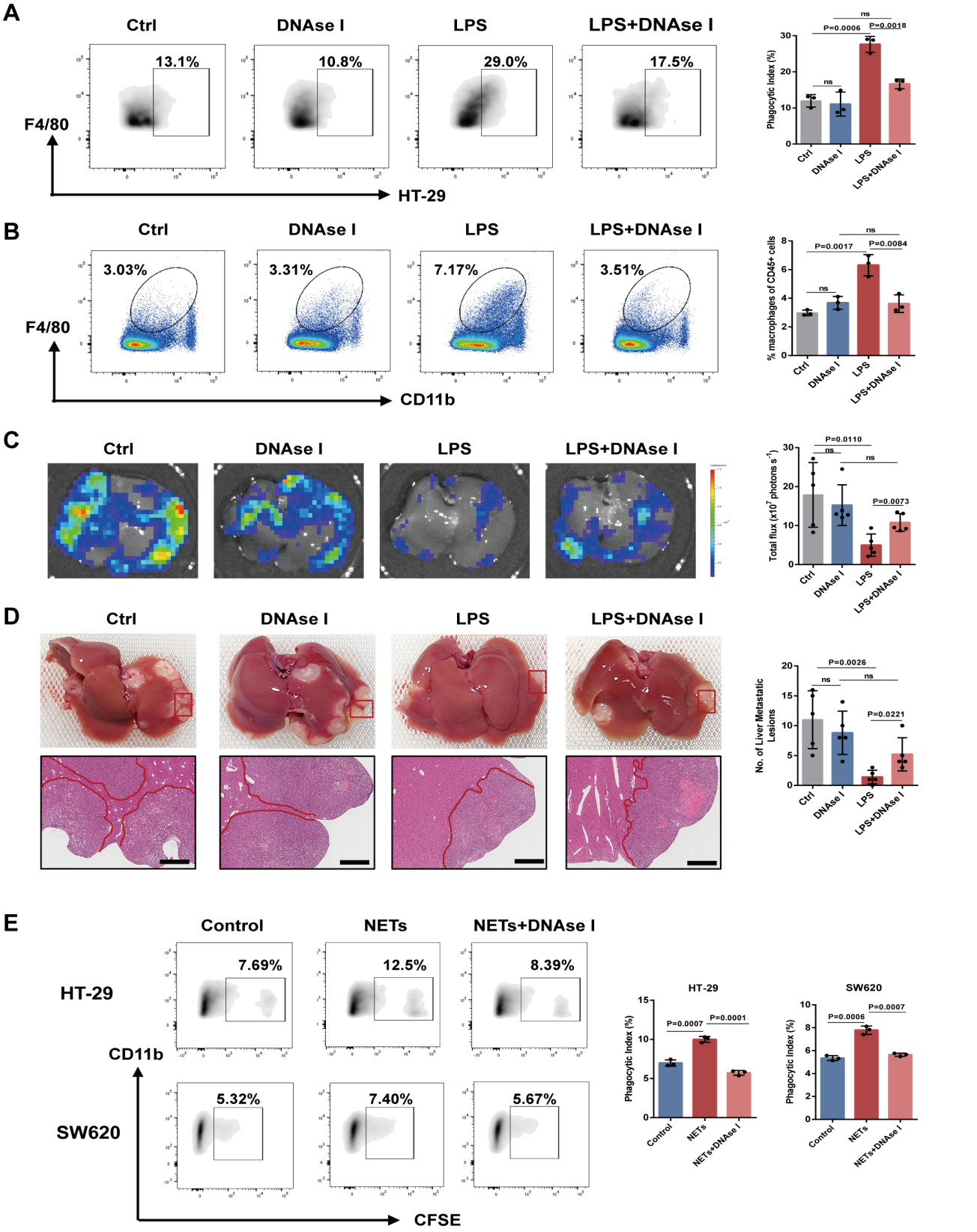

Figure 1 Neutrophil extracellular traps (NETs) enhance macrophage phagocytosis of tumor cells. (A) Flow cytometry showing carboxyfluorescein succinimidyl ester (CFSE)-labeled HT-29 cell phagocytosis by $CD11b^{+}F4/80^{+}$ macrophages in mouse livers at day 2 (n=3). (B) Flow cytometry of $CD11b^{+}F4/80^{+}$ macrophage infiltration in liver metastasis at day 2 (n=3). (C) Bioluminescence images and quantification of HT-29-luc cells in liver metastasis at day 2 (n=5). (D) Macroscopic and H&E staining of metastatic liver lesions at day 56 (n=5). (E) Phagocytosis of HT-29 and SW620 cells treated with NETs by THP-1 macrophages in vitro. Data are means±SEM of three independent experiments; Student's t-test. LPS, lipopolysaccharide; ns, not significant.

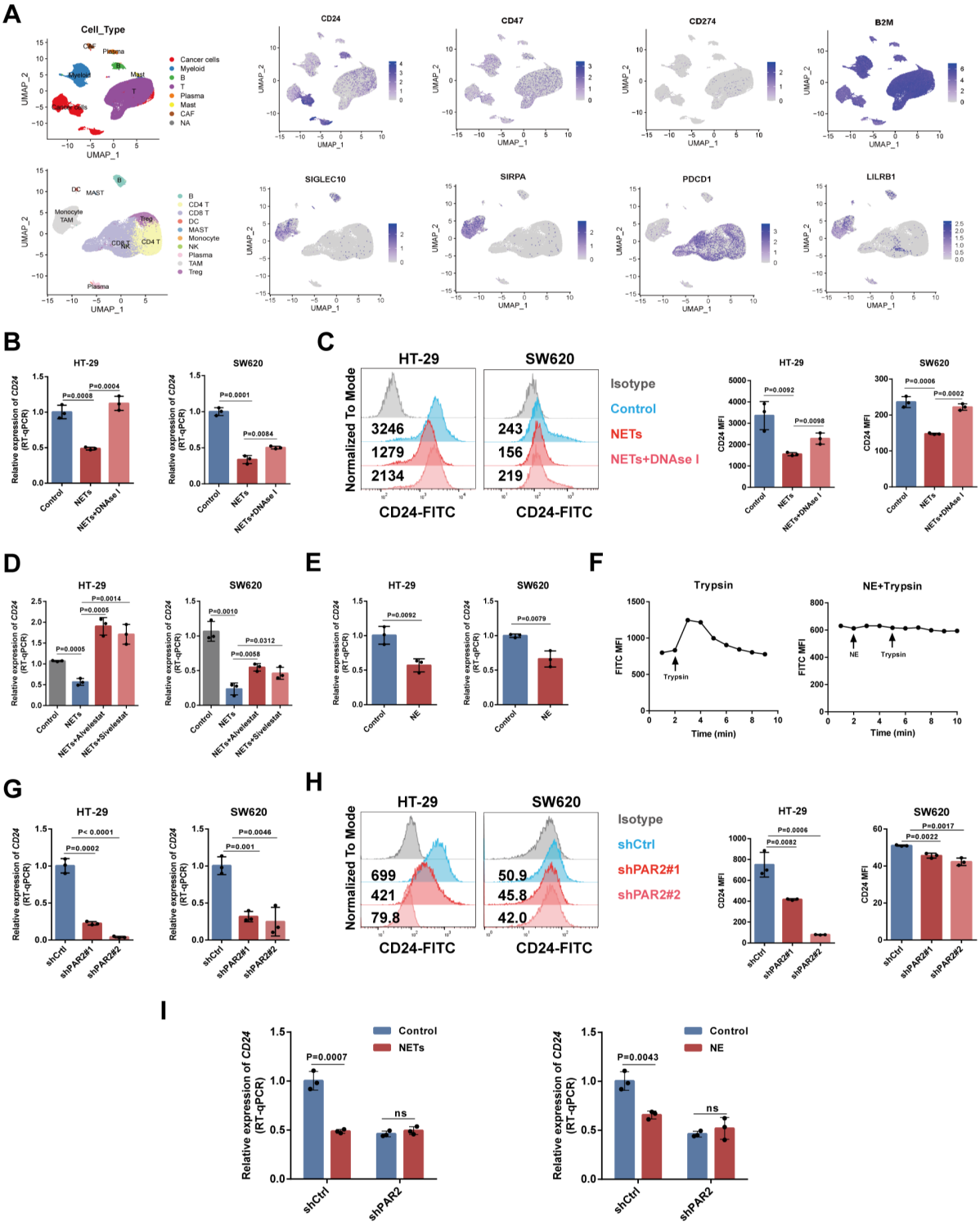

Figure 2 Neutrophil extracellular trap (NET)-derived elastase downregulates CD24 via protease-activated receptor 2 (PAR2) in colorectal cancer (CRC) cells. (A) Uniform Manifold Approximation and Projection plots of all cell clusters and immune cells from human CRC liver metastasis scRNA-seq with *CD24, CD274, B2M, CD47,* and their receptor genes overlaid (right). (B) CD24 mRNA expression in HT-29 and SW620 cells treated with NETs (RT-qPCR). (C) Flow cytometry analysis of CD24 expression in NET-treated HT-29 and SW620 cells, with median fluorescence intensity (MFI). (D) CD24 mRNA levels in cells treated with NETs and neutrophil elastase (NE) inhibitors (Alvelestat/Sivelestat) (RT-qPCR). (E) CD24 mRNA expression in NE-treated cells. (F) Ca^{2+} signals in HEK-293T cells treated with Trypsin and NE (flow cytometry). (G) CD24 mRNA expression in HT-29 and SW620 cells (shCtrl and shPAR2). (H) Flow cytometry analysis of CD24 expression in shCtrl and shPAR2 cells with MFI. (I) CD24 mRNA expression in shCtrl and shPAR2 cells treated with NETs or NE. Data are means±SEM of three independent experiments; Student's t-test. CAF, cancer-associated Fibroblast; Ca2+, calcium ion; DC, dendritic cell; FITC, fluorescein isothiocyanate; mRNA, messenger RNA; NK, natural killer; ns, not significant; RT-qPCR, reverse transcription-quantitative PCR; scRNA, single-cell RNA; TAM, tumor-associated macrophage; UMAP, Uniform Manifold Approximation and Projection.

PAR2-mediated NET-induced macrophage phagocytosis

To verify whether PAR2 functionally mediated NET-related phagocytosis, we investigated the effect of PAR2 deficiency on macrophage phagocytosis. First, we used flow cytometry to identify macrophages that had engulfed CFSE-labeled tumor cells. The percentage of $CD11b^{+}CSFE^{+}$ cells was significantly higher in shPAR2 groups than that in the control group, suggesting the enhanced engulfment of shPAR2 cancer cells by THP-1-derived TAMs or peripheral blood-derived TAMs (figure 3A and online supplemental figure 4A). This was supported by time-lapse live-cell microscopy-based phagocytosis assay labeling with pHrodo Deep Red, which showed red fluorescence only under acidic conditions, indicating the presence of phagolysosomes (figure 3B). Overexpression of CD24 completely blocked the phagocytosis enhancement caused by PAR2 deletion (figure 3C and online supplemental figure 4B, C), revealing that CD24 mediates PAR2-regulated macrophage phagocytosis in vitro. Furthermore, NETs failed to enhance macrophage phagocytosis in the cells' stable knockdown of PAR2 (figure 3D). This indicates that NET-induced macrophage phagocytosis is dependent on PAR2 in CRC cells.

PAR2 deficiency downregulated CD24 via miR-34a and miR-146a

As CD24 is a direct target of miR-34a and miR-146a,[30 31] we hypothesized that microRNAs (miRNAs) may mediate the regulation of CD24 expression by PAR2. We found that miR-34a and miR-146a were upregulated by PAR2 knockdown, as measured by the miRNA microarray (figure 4A), which was verified using RT-qPCR in different cells (online supplemental figure 5A). In addition, ectopic miR-34a or miR-146a expression decreased the CD24 mRNA levels, whereas their inhibitors increased CD24 expression (online supplemental figure 5B, C). Furthermore, in different cells, the decrease in CD24 expression caused by PAR2 deficiency was partially reversed by the inhibition of miR-34a or miR-146a expression alone (figure 4B), whereas combined inhibitors restored it almost completely (figure 4C,D). These results indicate that PAR2 deletion downregulates CD24 via miR-146a and miR-34a in CRC cells. Furthermore, treatment with NETs or NE also elevated the expression of both miRNAs (figure 4E). Combined miRNA inhibitors partly restore the expression of CD24 after its downregulation by NETs or NE (figure 4F). These data substantiate the claim that NET-derived NE decreases the CD24 expression via PAR2-regulated miRNAs.

PAR2 deficiency increased recruitment and promoted M1-like macrophage polarization

Because NETs were associated with an increased macrophage infiltration at the early stage of liver metastasis (figure 1), the effect of NET-treated cancer cells on macrophage infiltration was evaluated using an in vitro trans-well migration assay. First, conditioned medium from cancer cells with shPAR2 significantly enhanced the migration ability of THP-1 macrophages (online supplemental figure 6A). Analysis of mRNA microarray data revealed that *CSF1* and *CXCL1* were significantly enriched in shPAR2 HT-29 cells (online supplemental figure 6B). RT-qPCR and ELISA validated the upregulation and secretion of CSF1 and CXCL1 following PAR2 knockdown in HT-29 and SW620 cells (online supplemental figure 6C, D). Given the core effect of CSF-1 and CXCL1 on chemoattract and polarization of macrophages,[32 33] we explored macrophage polarization using the co-culture of CRC cells with THP-1-derived macrophages referred to as TAMs (online supplemental figure 6E). First, RNA-seq and RT-qPCR analyses showed that TAMs induced by shPAR2 cancer cells expressed higher levels of M1-featured genes, including *IL-12B, IL1A*, and *TNFA* (online supplemental figure 6F), while these genes were not expressed or not upregulated in CRC cells after co-culture. Cytokine analysis of the co-culture supernatant further confirmed high yields of proinflammatory cytokines by TAMs induced by shPAR2 cancer cells (online supplemental figure 6G). However, there was no change in the levels of M2-associated cytokines, such as IL-10, at the mRNA and protein levels. Consistent with the cytokine profile, flow cytometry analysis revealed an increase in the counts of $CD11b^{+}CD86^{+}$ M1-like TAMs, whereas the percentage of $CD11b^{+}CD206^{+}$ M2-like TAMs decreased after co-culture with shPAR2 cancer cells (online supplemental figure 6H). This indicates that PAR2 deficiency enhances the recruitment of macrophages and promotes M1-like macrophage polarization. Critically, the conditioned media from cancer cells treated with NETs or NE simulated the effect of shPAR2 cancer cells on macrophage migration (online supplemental figure 6I), production of CSF-1 and CXCL1 (online supplemental figure 6J). The results corroborate that NETs/NE upregulate macrophage chemokines and promote macrophage recruitment and M1 type polarization via PAR2 in vitro.

NETs regulated macrophage phagocytosis and liver metastasis through PAR2 in vivo

To verify whether NETs promote phagocytosis via PAR2 in vivo, we established the liver metastasis model with shPAR2 HT-29 cells with or without LPS-induced NETs. Concordant with the in vitro study, shPAR2 cells promoted macrophage phagocytosis and liver infiltration (figure 5A–C), accompanied by M1-like polarization of macrophages evidenced by flow cytometry and IF staining on day 2 after intrasplenic inoculation (online supplemental figure 7A). Notably, these phenomena were not observed at the endpoint (day 56) when the metastatic nodule had formed (online supplemental figure 7B, C). In addition, shPAR2 significantly suppressed cancer colonization on day 2 (figure 5D), followed by reduced

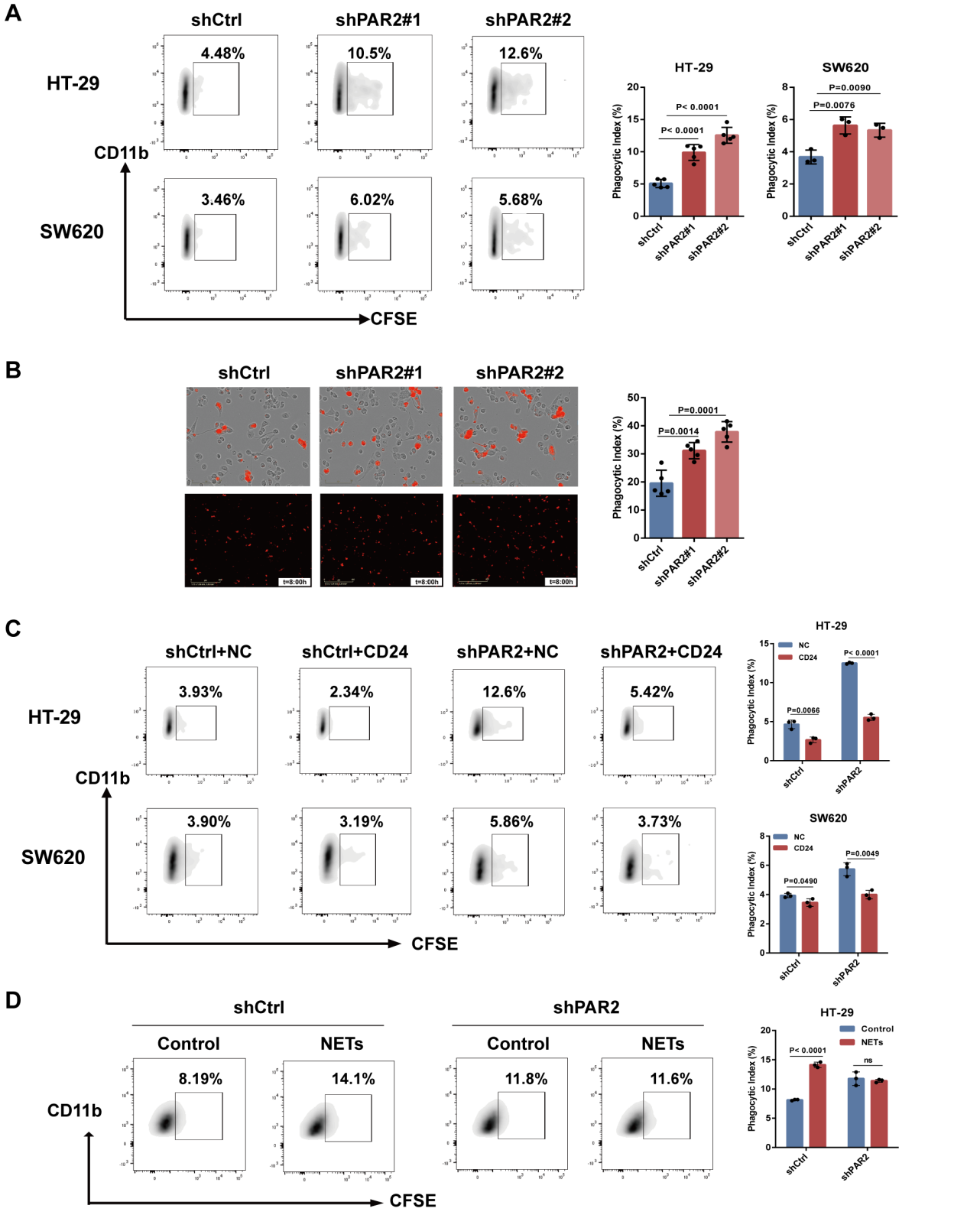

Figure 3 Protease-activated receptor 2 (PAR2)-mediated neutrophil extracellular trap (NET)-induced macrophage phagocytosis. (A) Representative images of flow cytometry analysis depicting the phagocytosis of HT-29 and SW620 cells (shCtrl and shPAR2) (left). The phagocytic index was measured (right). (B) Representative images for live-cell microscopy phagocytosis assays of tumor-associated macrophages and pHrodo Deep Red^{+} HT-29 cells (shCtrl and shPAR2), t=8:00 hours (left). The phagocytic index was measured (right). (C) HT-29 and SW620 cells (shCtrl and shPAR2) transfected with CD24-specific or control plasmids (NC and CD24). Representative images of flow cytometry analysis depicting the phagocytosis of HT-29 and SW620 cells. (D) Representative images of flow cytometry analysis depicting the phagocytosis of HT-29 cells (shCtrl and shPAR2) treated with NETs (left). The phagocytic index was measured (right). All data are mean±SEM of three independent experiments; Student's t-test. CFSE, carboxyfluorescein succinimidyl ester; NC, normal control.

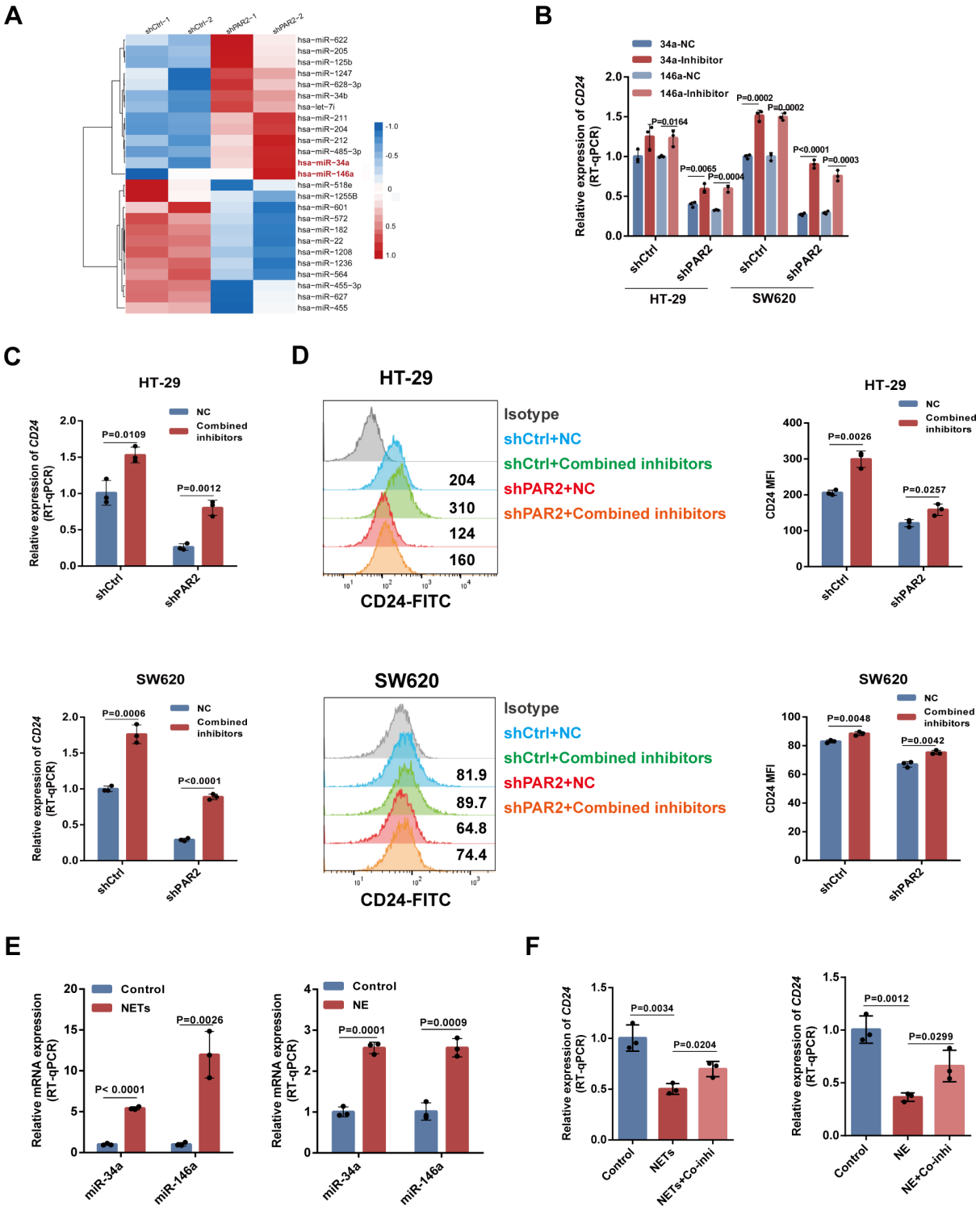

Figure 4 Protease-activated receptor 2 (PAR2) deficiency reduces CD24 expression through miR-34a and miR-146a. (A) Heatmap showing differentially expressed miRNAs between HT-29 cells (shCtrl and shPAR2) (top 25) detected by miRNA microarray. (B) HT-29 and SW620 cells (shCtrl and shPAR2) transfected with miR-34a and miR-146a inhibitors alone. (C, D) HT-29 and SW620 cells (shCtrl and shPAR2) simultaneously transfected with inhibitors of both miR-34a and miR-146a (Combined inhibitors). (C) Relative mRNA expression levels of CD24 in HT-29 and SW620 cells (shCtrl and shPAR2) examined using RT-qPCR. (D) Representative histogram of flow cytometry analyses for CD24 expression in HT-29 and SW620 cells (shCtrl and shPAR2) (left). Anti-CD24 mAb MFI was measured (right). (E) Relative mRNA expression levels of miR-34a and miR-146a in HT-29 cells treated with NETs or NE examined using RT-qPCR. (F) RT-qPCR analysis for assessing the relative mRNA expression levels of CD24 in HT-29 cells treated with NETs or NE that were simultaneously transfected with inhibitors of both miR-34a and miR-146a. All data are means±SEM of three independent experiments; Student's t-test. FITC, fluorescein isothiocyanate; MFI, mean fluorescence intensity; miRNA, microRNA; mRNA, messenger RNA; NC, normal control; NE, neutrophil elastase; NET, neutrophil extracellular trap; RT-qPCR, reverse transcription-quantitative PCR.

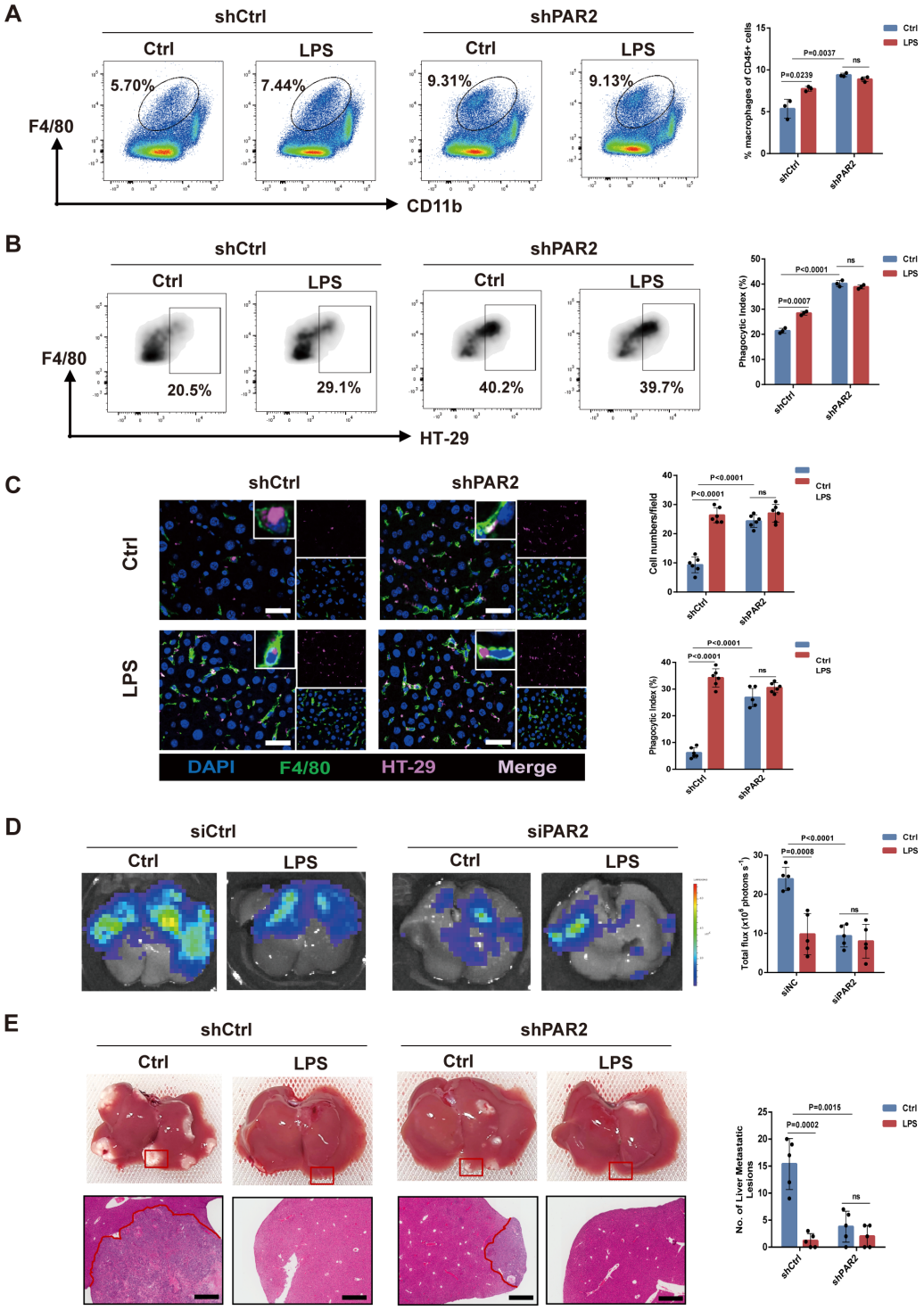

Figure 5 Neutrophil extracellular traps (NETs) regulate macrophage phagocytosis in vivo via PAR2 on tumor cells. (A–E) An experimental liver metastasis model induced by HT-29 cells (shCtrl and shPAR2) in lipopolysaccharide-induced NET model. (A) Flow cytometry analysis to assess $CD11b^{+}F4/80^{+}$ macrophage infiltration in the experimental liver metastasis model at day 2. Representative plot (left) and quantification (right) are shown (n=3). (B) Representative images of flow cytometry analysis depicting the phagocytosis of HT-29 cells in mouse livers (left) at day 2. The phagocytic index was measured (right) (n=3). (C) Immunofluorescence staining of the F4/80 of liver tissue sections obtained from representative mice induced by HT-29 cells (shCtrl and shPAR2) at day 2. Representative images showing F4/80 (green), pHrodo Deep Red^{+} HT-29 cells (pink), and DAPI (blue) (left). The phagocytic index was measured (right). Scale bar=50 µm. (D) Representative bioluminescence images of day 2 mouse livers engrafted with HT-29-luciferase cells (siNC and siPAR2) (left). Tumor cell numbers in mouse livers, as measured via bioluminescence (right) (n=5). (E) Representative macroscopic observation of metastatic liver tumor lesions (left) in the liver metastasis model and their quantification (right) at day 56 (n=5). H&E staining of metastatic liver tumor lesions; scale bar=1 mm. All data are mean±SEM of three independent experiments; Student's t-test. DAPI, dihydrochloride; GO, Gene Ontology; LPS, lipopolysaccharide; ns, not significant; PAR2, protease-activated receptor 2.

numbers of metastasis lesions at the end point (figure 5E), which is suggestive of the critical role of phagocytosis at the seeding step. Importantly, LPS-induced NET formation in the liver did not affect the shPAR2 cell-mediated enhancement of macrophage phagocytosis, infiltration, and subsequently, shPAR2 cell-mediated repression of early cancer cell colonization and metastasis; these effects were different from those of LPS-induced NET formation on shRNA control (shCtrl) cells (figure 5A–E). These findings indicate that NETs regulate macrophage phagocytosis and liver metastasis via PAR2 in vivo.

Correlation of the PAR2-CD24 axis with human CRC

To assess the correlation between PAR2 expression and macrophages, we first investigated PAR2 gene *F2RL1* expression at the single-cell level using scRNA-seq data from CRC liver metastases (GSE178318).[34] The cluster of cancer cells exhibited robust *F2RL1* expression, but no other cells, including myeloid cells, did so (figure 2A and online supplemental figure 8A, B). Subsequently, subcluster analysis for cancer cells was conducted (online supplemental figure 8C). Cancer cells were divided into *F2RL1*-high and *F2RL1*-low groups according to the percentage and expression levels of *F2RL1* (online supplemental figure 8D–F). Analysis of differentially expressed genes (DEGs) showed that *CD24* was one of the top five DEGs between *F2RL1*-high and *F2RL1*-low groups (figure 6A). Moreover, monocyte-related feature genes, such as mononuclear cell differentiation, myeloid leukocyte activation, and phagocytosis, were dramatically enriched in the *F2RL1*-low group (figure 6B). Additionally, RT-qPCR analysis of primary tumor tissue from 37 patients with CRC showed that PAR2 mRNA expression was negatively correlated with the expression of CD68 (encoding a macrophage marker) but positively correlated with that of CD206 (an M2 marker) (figure 6C). Moreover, CD24 mRNA expression was significantly correlated with PAR2 expression (figure 6D), while miR-34a and miR-146a expression was negatively correlated with PAR2 expression in CRC samples (figure 6E). Multiplex IHC staining to detect PAR2, CD24, and CD68 was performed using the CRC tissue array. PAR2 expression was inversely correlated with $CD68^+$ TAM infiltration and positively correlated with CD24 expression in cancer lesions (figure 6F).

As a negative regulator of PAR2 activity, NE was negatively associated with CD24 gene expression in primary tumor tissues of 37 patients with CRC (figure 6G). Finally, IHC staining in liver metastasis samples demonstrated that the region with higher NE expression in stroma showed lower CD24 expression in adjacent cancer cells while vice versa (figure 6H). Collectively, these results indicate that cancer cells may regulate macrophage infiltration and phagocytosis via the PAR2-CD24 axis in CRC metastasis. Neutrophil-derived NE may function as a negative regulator of PAR2 activity during liver metastasis.

PAR2 inhibitors enhanced anticancer effects of anti-EGFR antibody

PAR2 is not only the key molecule linking NETs and the antitumor effects of macrophages, but is also highly expressed in CRC-initiating cells,[28] strongly suggesting that PAR2 is an attractive therapeutic target for advanced CRC. Anti-EGFR mAb (CTX), used clinically in patients with advanced CRC, is an opsonizing antibody that stimulates antitumor immunity through antibody-dependent cellular phagocytosis (ADCP).[11 25 35] Therefore, we speculated that inhibition of PAR2 expression may enhance the therapeutic effects of CTX in CRC metastasis. The in vitro phagocytosis assay revealed that CTX alone enhanced phagocytosis, which was further enhanced by the combination with anti-CD24 mAb (figure 7A). Moreover, synergy between PAR2 deletion and CTX enhanced phagocytosis (figure 7B), indicating that inhibition of PAR2 expression enhances the antitumor effect of CTX in vitro. To determine whether combination treatment targets the early stages of liver metastasis, mice were initially treated with PAR2 inhibitor GB88 and a single dose of CTX immediately following the splenic injection of HT-29 cells (online supplemental figure 9A). The increase of miR-34a and miR-146a expression and reduction of CD24 expression in CRC cells by GB88 was verified (online supplemental figure 9B, C). Combination therapy drastically enhanced the phagocytosis of the macrophages (figure 7C) and inhibited cancer cell survival in the liver on day 2 after inoculation (figure 7D) and metastatic nodule formation at the end of the experiment, compared with either treatment alone (figure 7E). Therefore, the data suggest that the PAR2 inhibitor enhances the anticancer effect of EGFR antibody in vivo. The combined treatment may provide a distinguished therapeutic strategy against advanced CRC.

DISCUSSION

In the present study, we found that NETs prevented liver metastasis by promoting macrophage phagocytosis. NETs have attracted significant attention for their tumor-promoting effects.[13 36–38] We observed that NETs stimulated PD-L1 expression (data not shown), which has been reported previously and has been proposed as a tumor-promoting mechanism of NETs.[39–41] This is in line with the results of our study. However, PD-L1 appears not to prominently affect the phagocytosis of CRC cells by macrophages, which primarily mediate immune escape to T cells.[42] We believe that the timing of tumor cell colonization is crucial for NETs to exert antimetastasis effects. On arrival, CTCs face clearance by innate immune cells in the liver. On the first couple of days, neutrophils capture CTCs by releasing NETs, recruit M1-like macrophages, and enhance phagocytosis by suppressing “don’t eat me” molecules, consequently eliminating more

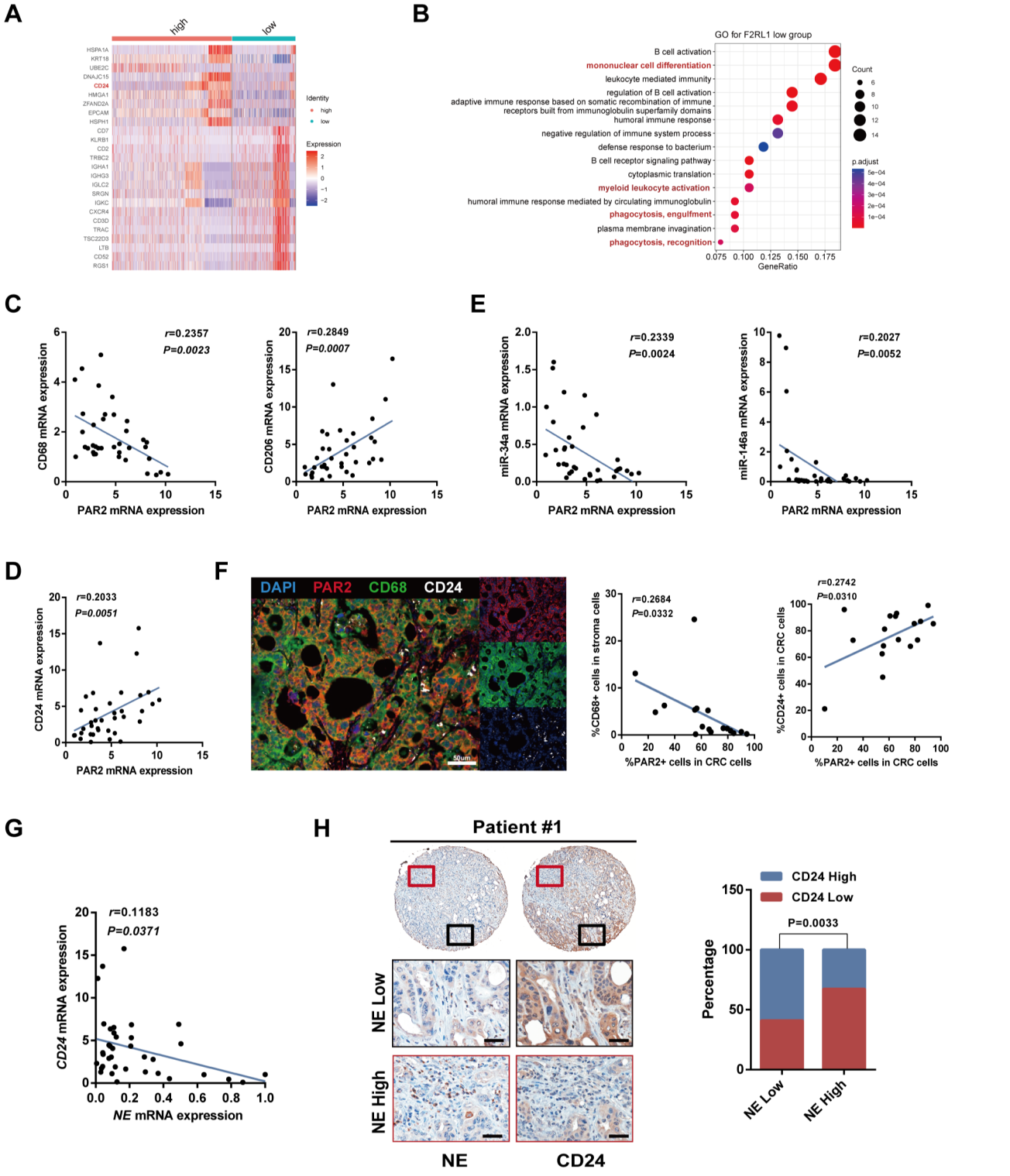

Figure 6 Correlation between protease-activated receptor 2 (PAR2) and CD24 expression in human colorectal cancer (CRC). (A) Heatmap showing the differentially expressed genes between *F2RL1*-high and *F2RL1*-low group cancer cells (top 25) from scRNA-seq data of patients with CRC liver metastasis (GSE178318). (B) GO analysis showing biological function terms for genes upregulated in the *F2RL1*-low group. (C–E) Correlation between PAR2 mRNA expression levels and the expression of CD68, CD206, CD24, miR-34a, and miR-146a of tumor tissues in patients with CRC (n=37); two-tailed Pearson test. (F) Multiplex immunohistochemistry (IHC) staining of CD24, CD68, and PAR2 in human metastatic CRC tumor tissues; scale bar=100 µm. Correlation between percentage of $PAR2^+$ and $CD68^+$ cells (left) and $CD24^+$ cells (right) in patients with CRC; two-tailed Pearson test; n=17. (G) Correlation between neutrophil elastase (NE) mRNA expression levels and CD24 expression of tumor tissues in patients with CRC (n=37); two-tailed Pearson test. (H) IHC staining of NE and CD24 in human metastatic CRC tumor tissues; scale bar=100 µm (left). Correlation between the percentage of NE and CD24 expression (n=32). mRNA, messenger RNA; scRNA, single-cell RNA.

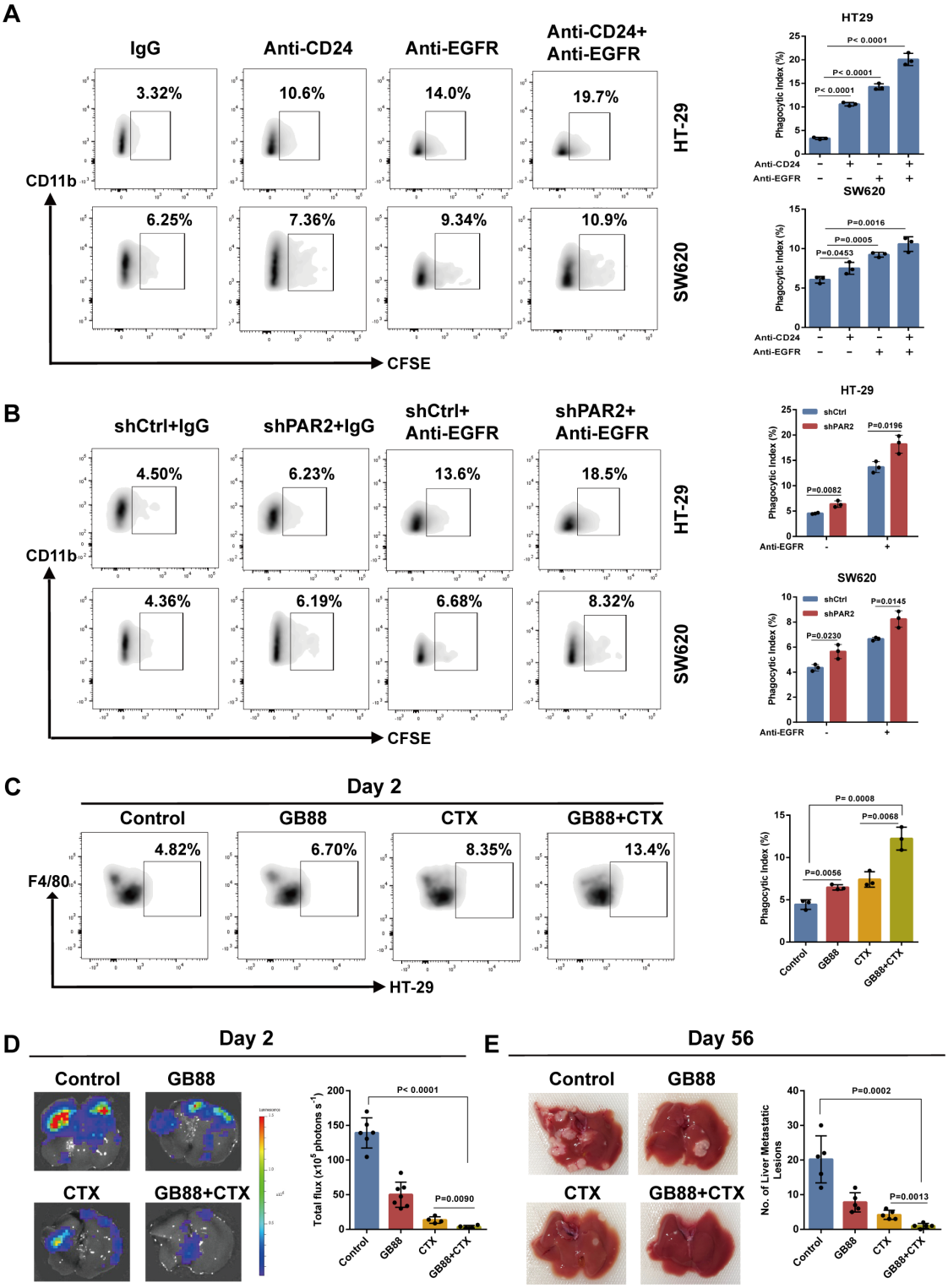

Figure 7 Inhibition of protease-activated receptor 2 (PAR2) expression enhances the anticancer effects of anti-EGFR antibodies. (A) Representative images of flow cytometry analysis depicting the phagocytosis of HT-29 and SW620 cells treated with anti-CD24, anti-EGFR mAb (cetuximab (CTX)), or both anti-CD24 and anti-EGFR mAb, compared with the IgG control. (B) Representative images of flow cytometry analysis depicting the phagocytosis of HT-29 and SW620 cells (shCtrl and shPAR2) treated with the IgG control or anti-EGFR mAb. (C–E) HT-29 cell-induced liver metastasis of colorectal cancer (CRC) in mice. (C) Representative images of flow cytometry analysis depicting the phagocytosis of pHrodo Deep Red^{+} HT-29 cells in mouse livers (left) at 2 days. The phagocytic index was measured (right). (D) Representative bioluminescence images of mouse livers at 2 days (left). Tumor cell numbers of each group in mouse livers as measured via bioluminescence (right); (Control and GB88 groups, n=6; cetuximab (CTX) and GB88+CTX groups, n=4). (E) Representative macroscopic observation of metastatic liver tumor lesions (left) and their quantification (right) at 56 days (n=5). All data are means±SEM of three independent experiments; Student's t-test. CFSE, carboxyfluorescein succinimidyl ester; IgG, immunoglobulin G; mAb, monoclonal antibody.

seeding cells. During this phase, short-term phagocytosis-promoting therapy can achieve a significant long-term inhibitory effect on metastasis, which is sufficient to demonstrate the importance of this time point. Moreover, a most recent study has demonstrated that NETs induced by chemotherapy can kill tumor cells in CRC.[43] The authors suggest that the induction of a large amount of NETs release by chemotherapy may be the key to this antitumor effect. Therefore, exploring how to control and promote the antitumor effect of NETs will not only deepen the understanding of the mechanism of tumor progression but also provide novel strategies for cancer therapy in the future.

NE is the most abundant serine protease released by mature neutrophils through degranulation and NET formation.[44] Here, we revealed a novel function of NE in regulating phagocytosis during liver metastasis. NE irreversibly cleaves the extracellular N-terminus of PAR2 and prevents canonical activation by other proteases like trypsin.[27] Different lines of evidence, including ours, have shown PAR2 to be strongly associated with poor prognosis in patients with CRC.[27 28] In addition, cancer stem-like cells in CRC highly express PAR2, which promotes self-renewal, survival, and cell proliferation.[28 29 45] All of these are the characteristics that are required for successful metastasis seeding. Besides the innate immunomodulatory effects shown in this study, PAR2 is also involved in the regulation of adaptive immunity through type I interferon.[46] Collectively, PAR2 is a key molecule for regulating stemness and immune evasion during the metastatic seeding process. Inhibition of PAR2 expression significantly attenuated liver metastasis in vivo, suggesting that PAR2 is a potential target for advanced CRC therapy. More importantly, PAR2 blockade significantly synergized with EGFR-blocking antibody CTX, which is one of the few drugs clinically used in CRC, by suppressing the expression of the phagocytic checkpoint CD24.

Phagocytic checkpoints are attractive targets for cancer immunotherapy, and their blockade significantly improves the efficacy of antibody therapy. For example, anti-CD47 mAbs exhibit a synergistic effect with anti-CD20 rituximab in lymphoma, anti-HER2 trastuzumab in breast cancer, and anti-EGFR CTX (NCT02953782) in CRC.[6] These synergistic responses are partly based on inducing ADCP via the "eat me" signaling activated by the binding of the antibody Fc region to FcγR on macrophages.[35] However, due to their strong adverse effects, clinical trials of CD47-blocking antibodies have been discontinued or restrained.[47 48] Compared with CD47, CD24 is more selectively expressed by cancer cells, but not by the hematologic and immune systems.[25] In this study, we demonstrated that CD24 has immunotherapeutic significance in CRC. Moreover, NETs or PAR2 deficiency specifically reduce CD24 expression in a miRNA-dependent manner, but not CD47. Notably, co-culture with macrophages drastically increased CD47 expression on cancer cells; however, it was considerably lower in shPAR2 cells than that in the control cells (data not shown). This result suggests an unexplored effect of PAR2 signaling on macrophage-induced CD47 expression.

We demonstrated that NETs promote phagocytosis ex vivo and in vivo with an LPS-induced NET model. However, the NETs studied here were all released from healthy neutrophils. Because the primary tumor is capable of modulating neutrophil development and phenotypes systemically through tumor-derived signaling,[49] whether the NETs produced at different stages of tumors are consistent in regulating phagocytosis should be studied in the future. Moreover, the immune cell composition of a metastatic organ may determine the function of neutrophils on metastasis. For example, neutrophils could restrict metastatic cell growth in the lung in the absence of NK cells, while they show protumorigenic functions in the presence of NK cells.[50] Although BALB/c nude mice, which lack T and NK cells, are useful for studying the relationship between neutrophils and macrophages, the role of NK cells in these interactions can only be determined using immunocompetent mice, which we suggest for future studies.

In summary, NE inactivated PAR2 canonical signaling and promoted phagocytosis by downregulating CD24, which functions as a phagocytic checkpoint in CRC liver metastasis. PAR2 is a key node that manipulates the ability to initiate tumor formation and evade immune surveillance. Therefore, PAR2 inhibitors combined with CTX may provide a novel therapeutic strategy against advanced CRC.

Author affiliations
[1]State Key Laboratory of Molecular Oncology, National Cancer Center/National Clinical Research Center for Cancer/Cancer Hospital, Chinese Academy of Medical Sciences and Peking Union Medical College, Beijing, Beijing, China
[2]Department of Pathology and Resident Training Base, National Cancer Center/National Clinical Research Center for Cancer/Cancer Hospital, Chinese Academy of Medical Sciences and Peking Union Medical College, Beijing, Beijing, China
[3]Department of Immunology, National Cancer Center/National Clinical Research Center for Cancer/Cancer Hospital, Chinese Academy of Medical Sciences and Peking Union Medical College, Chaoyang District, Liaoning, China
[4]State Key Lab of Molecular Oncology, National Cancer Center/National Clinical Research Center for Cancer/Cancer Hospital, Chinese Academy of Medical Sciences and Peking Union Medical College, Chaoyang District, Liaoning, China
[5]Department of Injury and Repair, Beijing Neurosurgical Institute, Capital Medical University, Beijing, Beijing, China

Acknowledgements We would like to thank Mr Tao Xu for technical support on flow cytometry and thank Editage (www.editage.cn) for their assistance with English language editing.

Contributors YL: Conceptualization, Methodology, Investigation, and Writing Original Draft. JM: Validation, Formal Analysis, and Data Curation. YM, YL, YW, JY, FZ, KC, BW, XHZ and XLZ: Methodology and Resources. HW: Conceptualization, Resources, Writing—Review and Editing, Supervision, Funding Acquisition, and Project Administration. HW is the guarantor.

Funding This work was supported by the National Nature Science Foundation of China (22193034, 81970467, 82203229), CAMS Innovation Fund for Medical Sciences (CIFMS; 2022-I2M-1-009, 2021-I2M-1-067), State Key Laboratory of Molecular Oncology, and Shenzhen Science and Technology Program (JCYJ20220531094005012).

Competing interests None declared.

Patient consent for publication Not applicable.

Ethics approval The present study was performed at the Chinese Academy of Medical Sciences, Cancer Hospital (Beijing, China). Procedures used for the collection and analyses of human samples were approved by the ethics committee of the Chinese Academy of Medical Sciences, Cancer Hospital (Approval No. NCC2023C-459). All animal experiments were performed based on the guidelines stipulated by the National Institutes of Health Guide for the Care and Use of Laboratory Animals and approved by the Ethics Committee of the Chinese Academy of Medical Sciences, Cancer Hospital (Approval No. NCC2023A126).

Provenance and peer review Not commissioned; externally peer reviewed.

Data availability statement Data are available in a public, open access repository. Data are available in a public, open access repository. Data are available upon reasonable request. All data relevant to the study are included in the article or uploaded as supplementary information. The public single-cell RNA-sequencing data sets used in this research were obtained from the data sets GSE178318[34] was retrieved from the Gene Expression Omnibus (GEO) database (https://www.ncbi.nlm.nih.gov/geo/). MicroRNAs sequencing data were acquired from the study conducted by YL *et al*. All data are available on request from the corresponding author (HW, National Cancer Center/National Clinical Research Center for Cancer/Cancer Hospital, Email: hongyingwang@cicams.ac.cn).

ORCID iDs
Kun Chen http://orcid.org/0000-0003-3146-2577
Hongying Wang http://orcid.org/0000-0001-8443-3839

REFERENCES

1 Massagué J, Obenauf AC. Metastatic colonization by circulating tumour cells. *Nature New Biol* 2016;529:298–306.
2 Tsilimigras DI, Brodt P, Clavien P-A, *et al*. Liver metastases. *Nat Rev Dis Primers* 2021;7:27.
3 Keirsse J, Van Damme H, Geeraerts X, *et al*. The role of hepatic macrophages in liver metastasis. *Cell Immunol* 2018;330:202–15.
4 Feng M, Jiang W, Kim BYS, *et al*. Phagocytosis checkpoints as new targets for cancer immunotherapy. *Nat Rev Cancer* 2019;19:568–86.
5 Klein CA. Cancer progression and the invisible phase of metastatic colonization. *Nat Rev Cancer* 2020;20:681–94.
6 Advani R, Flinn I, Popplewell L, *et al*. CD47 Blockade by Hu5F9-G4 and Rituximab in Non-Hodgkin's Lymphoma. *N Engl J Med* 2018;379:1711–21.
7 Shibata T. Diverse Molecular Mechanisms for Immune Evasion in Gastrointestinal Cancer. *Gan To Kagaku Ryoho* 2022;49:243–7.
8 Jalil AR, Andrechak JC, Discher DE. Macrophage checkpoint blockade: results from initial clinical trials, binding analyses, and CD47-SIRPα structure-function. *Antib Ther* 2020;3:80–94.
9 Gordon SR, Maute RL, Dulken BW, *et al*. PD-1 expression by tumour-associated macrophages inhibits phagocytosis and tumour immunity. *Nature New Biol* 2017;545:495–9.
10 Majeti R, Chao MP, Alizadeh AA, *et al*. CD47 is an adverse prognostic factor and therapeutic antibody target on human acute myeloid leukemia stem cells. *Cell* 2009;138:286–99.
11 Barkal AA, Weiskopf K, Kao KS, *et al*. Engagement of MHC class I by the inhibitory receptor LILRB1 suppresses macrophages and is a target of cancer immunotherapy. *Nat Immunol* 2018;19:76–84.
12 Granot Z, Henke E, Comen EA, *et al*. Tumor entrained neutrophils inhibit seeding in the premetastatic lung. *Cancer Cell* 2011;20:300–14.
13 Cools-Lartigue J, Spicer J, McDonald B, *et al*. Neutrophil extracellular traps sequester circulating tumor cells and promote metastasis. *J Clin Invest* 2013;123:3446–58.
14 Najmeh S, Cools-Lartigue J, Rayes RF, *et al*. Neutrophil extracellular traps sequester circulating tumor cells via β1-integrin mediated interactions. *Int J Cancer* 2017;140:2321–30.
15 Castanheira FVS, Kubes P. Neutrophils and NETs in modulating acute and chronic inflammation. *Blood* 2019;133:2178–85.
16 Demkow U. Molecular Mechanisms of Neutrophil Extracellular Trap (NETs) Degradation. *Int J Mol Sci* 2023;24:4896.
17 Monteith AJ, Miller JM, Maxwell CN, *et al*. Neutrophil extracellular traps enhance macrophage killing of bacterial pathogens. *Sci Adv* 2021;7:eabj2101.
18 Kalbasi A, Ribas A. Tumour-intrinsic resistance to immune checkpoint blockade. *Nat Rev Immunol* 2020;20:25–39.
19 Song W, Shen L, Wang Y, *et al*. Synergistic and low adverse effect cancer immunotherapy by immunogenic chemotherapy and locally expressed PD-L1 trap. *Nat Commun* 2018;9:2237.
20 Yang L-Y, Luo Q, Lu L, *et al*. Increased neutrophil extracellular traps promote metastasis potential of hepatocellular carcinoma via provoking tumorous inflammatory response. *J Hematol Oncol* 2020;13:3.
21 Valk PJM, Verhaak RGW, Beijen MA, *et al*. Prognostically useful gene-expression profiles in acute myeloid leukemia. *N Engl J Med* 2004;350:1617–28.
22 Zhang X, Fang Q, Ma Y, *et al*. Protease activated receptor 2 mediates tryptase-induced cell migration through MYO10 in colorectal cancer. *Am J Cancer Res* 2019;9:1995–2006.
23 Miksa M, Komura H, Wu R, *et al*. A novel method to determine the engulfment of apoptotic cells by macrophages using pHrodo succinimidyl ester. *J Immunol Methods* 2009;342:71–7.
24 Kilkenny C, Browne WJ, Cuthill IC, *et al*. Improving bioscience research reporting: the ARRIVE guidelines for reporting animal research. *PLoS Biol* 2010;8:e1000412.
25 Barkal AA, Brewer RE, Markovic M, *et al*. CD24 signalling through macrophage Siglec-10 is a target for cancer immunotherapy. *Nature New Biol* 2019;572:392–6.
26 Ramachandran R, Mihara K, Chung H, *et al*. Neutrophil elastase acts as a biased agonist for proteinase-activated receptor-2 (PAR2). *J Biol Chem* 2011;286:24638–48.
27 Peach CJ, Edgington-Mitchell LE, Bunnett NW, *et al*. Protease-activated receptors in health and disease. *Physiol Rev* 2023;103:717–85.
28 Ma Y, He L, Zhao X, *et al*. Protease activated receptor 2 signaling promotes self-renewal and metastasis in colorectal cancer through β-catenin and periostin. *Cancer Lett* 2021;521:130–41.
29 Ma Y, Bao-Han W, Lv X, *et al*. MicroRNA-34a Mediates the Autocrine Signaling of PAR2-Activating Proteinase and Its Role in Colonic Cancer Cell Proliferation. *PLoS ONE* 2013;8:e72383.
30 Ghuwalewala S, Ghatak D, Das S, *et al*. MiRNA-146a/AKT/β-Catenin Activation Regulates Cancer Stem Cell Phenotype in Oral Squamous Cell Carcinoma by Targeting CD24. *Front Oncol* 2021;11:651692.
31 Muppala S, Mudduluru G, Leupold JH, *et al*. CD24 induces expression of the oncomir miR-21 via Src, and CD24 and Src are both post-transcriptionally downregulated by the tumor suppressor miR-34a. *PLoS One* 2013;8:e59563.
32 Pyonteck SM, Akkari L, Schuhmacher AJ, *et al*. CSF-1R inhibition alters macrophage polarization and blocks glioma progression. *Nat Med* 2013;19:1264–72.
33 Wu H, Jiang N, Li J, *et al*. Tumor cell SPTBN1 inhibits M2 polarization of macrophages by suppressing CXCL1 expression. *J Cell Physiol* 2024;239:97–111.
34 Che L-H, Liu J-W, Huo J-P, *et al*. A single-cell atlas of liver metastases of colorectal cancer reveals reprogramming of the tumor microenvironment in response to preoperative chemotherapy. *Cell Discov* 2021;7:80.
35 Bakalar MH, Joffe AM, Schmid EM, *et al*. Size-Dependent Segregation Controls Macrophage Phagocytosis of Antibody-Opsonized Targets. *Cell* 2018;174:131–42.
36 Zhan X, Wu R, Kong X, *et al*. Elevated neutrophil extracellular traps by HBV-mediated S100A9-TLR4/RAGE-ROS cascade facilitate the growth and metastasis of hepatocellular carcinoma. *Cancer Commun* 2023;43:225–45.
37 Shinde-Jadhav S, Mansure JJ, Rayes RF, *et al*. Role of neutrophil extracellular traps in radiation resistance of invasive bladder cancer. *Nat Commun* 2021;12:2776.
38 Song M, Zhang C, Cheng S, *et al*. DNA of Neutrophil Extracellular Traps Binds TMCO6 to Impair CD8+ T-cell Immunity in Hepatocellular Carcinoma. *Cancer Res* 2024;84:1613–29.
39 Kaltenmeier C, Yazdani HO, Morder K, *et al*. Neutrophil Extracellular Traps Promote T Cell Exhaustion in the Tumor Microenvironment. *Front Immunol* 2021;12:785222.

40 Fang Q, Stehr AM, Naschberger E, *et al*. No NETs no TIME: Crosstalk between neutrophil extracellular traps and the tumor immune microenvironment. *Front Immunol* 2022;13:1075260.
41 Teijeira A, Garasa S, Ochoa MC, *et al*. IL8, Neutrophils, and NETs in a Collusion against Cancer Immunity and Immunotherapy. *Clin Cancer Res* 2021;27:2383–93.
42 Shan J, Han D, Shen C, *et al*. Mechanism and strategies of immunotherapy resistance in colorectal cancer. *Front Immunol* 2022;13:1016646.
43 Li Y, Wu S, Zhao Y, *et al*. Neutrophil extracellular traps induced by chemotherapy inhibit tumor growth in murine models of colorectal cancer. *J Clin Invest* 2024;134.
44 Collins MS, Imbrogno MA, Kopras EJ, *et al*. Heterogeneity in Neutrophil Extracellular Traps from Healthy Human Subjects. *Int J Mol Sci* 2023;25:525.
45 Li W, Ma Y, He L, *et al*. Protease-activated receptor 2 stabilizes Bcl-xL and regulates EGFR-targeted therapy response in colorectal cancer. *Cancer Lett* 2021;517:14–23.
46 Ma J, Liu Y, Yuan J, *et al*. Bcl-xL mediates interferon-beta secretion by protease-activated receptor 2 deficiency through the mitochondrial permeability transition pore in colorectal cancer metastasis. *Cancer Lett* 2024;580:216483.
47 Zhang W, Huang Q, Xiao W, *et al*. Advances in Anti-Tumor Treatments Targeting the CD47/SIRPα Axis. *Front Immunol* 2020;11:18.
48 Yang Y, Yang Z, Yang Y. Potential Role of CD47-Directed Bispecific Antibodies in Cancer Immunotherapy. *Front Immunol* 2021;12:686031.
49 Wang J-L, Li X, Fan J-R, *et al*. Integrity of the editing and publishing process is the basis for improving an academic journal's Impact Factor. *World J Gastroenterol* 2022;28:6168–202.
50 Li P, Lu M, Shi J, *et al*. Dual roles of neutrophils in metastatic colonization are governed by the host NK cell status. *Nat Commun* 2020;11:4387.